Langmuir

Article

pubs.acs.org/Langmuir

Mechanisms of Molecular Permeation through Nanoporous Graphene Membranes

Chengzhen Sun,[†,‡] Michael S. H. Boutilier,[†] Harold Au,[†] Pietro Poesio,[§] Bofeng Bai,[‡] Rohit Karnik,[†] and Nicolas G. Hadjiconstantinou*[,†]

[†]Department of Mechanical Engineering, Massachusetts Institute of Technology, Cambridge, Massachusetts 02139, United States
[‡]State Key Laboratory of Multiphase Flow in Power Engineering, Xi'an Jiaotong University, Xi'an, Shaanxi 710049, China
[§]Department of Mechanical and Industrial Engineering, University of Brescia, Brescia 25123, Italy

Supporting Information

ABSTRACT: We present an investigation of molecular permeation of gases through nanoporous graphene membranes via molecular dynamics simulations; four different gases are investigated, namely helium, hydrogen, nitrogen, and methane. We show that in addition to the direct (gas-kinetic) flux of molecules crossing from the bulk phase on one side of the graphene to the bulk phase on the other side, for gases that adsorb onto the graphene, significant contribution to the flux across the membrane comes from a surface mechanism by which molecules cross after being adsorbed onto the graphene surface. Our results quantify the relative contribution of the bulk and surface mechanisms and show that the direct flux can be described reasonably accurately using kinetic theory, provided the latter is appropriately modified assuming steric molecule−pore interactions, with gas molecules behaving as hard spheres of known kinetic diameters. The surface flux is negligible for gases that do not adsorb onto graphene (e.g., He and H_2), while for gases that adsorb (e.g., CH_4 and N_2) it can be on the order of the direct flux or larger. Our results identify a nanopore geometry that is permeable to hydrogen and helium, is significantly less permeable to nitrogen, and is essentially impermeable to methane, thus validating previous suggestions that nanoporous graphene membranes can be used for gas separation. We also show that molecular permeation is strongly affected by pore functionalization; this observation may be sufficient to explain the large discrepancy between simulated and experimentally measured transport rates through nanoporous graphene membranes.

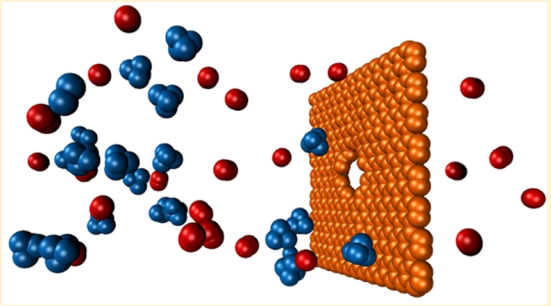

INTRODUCTION

Graphene[1,2] is a two-dimensional one-atom-thick sheet of sp^2-bonded carbon atoms packed in a honeycomb crystal lattice, which has good chemical stability,[3] excellent thermal conductance,[4,5] good mechanical strength,[6] and remarkable electronic properties.[7] Although pristine graphene is impermeable to gases,[8] nanoporous graphene (NPG), a graphene sheet featuring nanopores, has been proposed as a very promising size-selective gas separation membrane. Computational simulations and experiments[9−14] suggest that NPG can exhibit high permeance and selectivity exceeding those of existing state-of-the-art membranes by orders of magnitude. Methods for graphene fabrication,[15−18] transfer to porous substrates,[19−21] and pore generation[11,22−27] in the graphene sheet are currently being developed, making industrial-scale NPG-based gas separation membranes a future possibility. NPG has also shown promise for applications in water desalination,[28−31] isotope separation,[32−34] DNA sequencing,[35,36] and hydrogen storage,[37] among others.

Permeability is one of the most important characteristics of gas separation membranes because membranes with higher permeability can achieve separation using lower pressure differences and/or smaller membrane areas. Although some research has been conducted on gas separation by NPG membranes, little is known about the mechanisms by which molecules permeate graphene. Recently, it was reported by Du et al.[9] that for pores moderately larger than the nitrogen kinetic diameter the permeation rate of nitrogen exceeded that of hydrogen, while for significantly larger pores the flux of both gases was only weakly dependent on the pore area. They attributed the higher nitrogen flux to the adsorption of nitrogen molecules on the membrane surface. Even though the particular calculations of Du et al.[9] overstate the contribution of this phenomenon, molecular adsorption on the graphene membrane has been verified by other studies using molecular simulations.[38,39] This transport mode was included in the calculations by Drahushuk and Strano,[40] who developed a model for gas permeability through graphene membranes by identifying five rate-limiting steps. More recently, Liu et al.[14] used molecular dynamics (MD) simulations to calculate the

Received: October 14, 2013
Revised: December 20, 2013
Published: December 23, 2013

flux of molecular hydrogen across a graphene membrane with pores functionalized by nitrogen and hydrogen atoms. They reported a permeance in the range 1×10^5–4×10^5 GPU (gas permeation unit, 1 GPU = 3.35×10^{-10} mol/(s m^2 Pa)), which is in qualitative agreement with our simulations (their simulations were performed at a smaller pore density and considered a smaller pore than the pores studied here). In a separate publication,[13] they found pore structures that can separate carbon dioxide from nitrogen with a selectivity of 300 and exhibit CO_2 permeance on the order of 10^5 GPU.

Koenig et al.[11] used a pressurized blister test and mechanical resonance to measure the transport of a variety of gases (H_2, CO_2, Ar, N_2, CH_4, and SF_6) through nanopores, created by ultraviolet-induced oxidative etching, in micrometer-sized graphene membranes. Their measurements also showed that in some cases the flux of bigger molecules exceeded that of smaller molecules (e.g., CH_4 vs N_2). Shan et al.[38] elucidated the effects of chemical functionalization of the graphene sheet and pore rim on the separation of CO_2/N_2 and found that functionalization of the graphene sheet increased the adsorption of CO_2, while functionalization of the pore rim significantly improved the CO_2/N_2 selectivity.

In summary, the permeation of molecules through NPG membranes is related not only to transport rates to the surface but also to molecular adsorption on the graphene sheet, as well as chemical functionalization of the graphene sheet and pores. However, the extent of these different effects—in particular, steric exclusion versus surface adsorption and chemical functionalization—and how the transport of gas molecules through nanopores in graphene compares to that predicted by the kinetic theory of gases describing flow of an ideal gas through an aperture remains unclear.

In this paper, we perform MD simulations of transport across NPG membranes to systematically study the dependence of transport rates across the membrane on molecular size as well as surface adsorption. By decomposing the total flux across a pore into a direct (gas-phase) flux and a surface flux, we show that the surface flux can be of the same magnitude or even exceed the direct flux for molecules that strongly adsorb onto the graphene surface. We also show that the direct flux can be predicted by kinetic theory with reasonable accuracy, provided the finite size of molecules is taken into account. The resulting kinetic model not only enables the estimation of direct flux without costly molecular simulations but also serves as a means for validating molecular simulation results that to date have been surprisingly inconsistent. Finally, we attempt to reconcile the discrepancy between molecular simulation and experimental results by exploring the effects of pore functionalization on the membrane permeance and compare with existing experimental results.

SIMULATION METHOD

In order to obtain low-uncertainty estimates of molecular transport rates, we use classical MD simulations, which due to their small computational cost (compared to quantum mechanical calculations) allow the simulation of a large number of molecular trajectories without requiring excessive computational resources. For the temperatures of interest here, we expect quantum effects to be small.[32−34]

We investigate the molecular permeation of four different gases (He, H_2, N_2, and CH_4) through NPG membranes. Our simulations were performed using LAMMPS (Large-scale Atomic/Molecular Massively Parallel Simulator)[41] on the

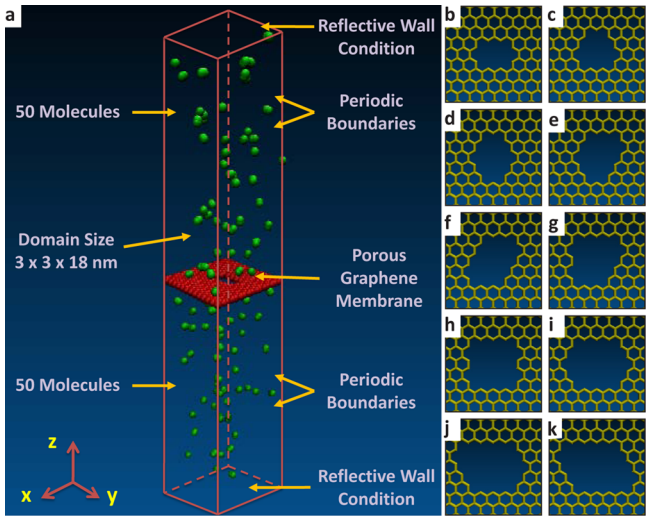

Figure 1. Simulation system and nanopore structures. (a) Simulation domain. (b–k) Structures of the nanopores employed in our simulation. The pores are named by the number of the graphene ring units removed or partially opened, i.e., (b) P-10, (c) P-12, (d) P-14, (e) P-16, (f) P-18, (g) P-20, (h) P-22, (i) P-24, (j) P-26, and (k) P-28.

"unit-cell" geometry shown in Figure 1a, in which a square graphene membrane of area $A_s = 3 \times 3$ nm^2 divides the simulation box of height 18 nm into two chambers of equal volume, with each chamber initially containing 50 molecules. Reflective boundary conditions were applied in the z-direction of the simulation box (normal to the graphene plane). Periodic boundary conditions were applied in the other two directions (x and y). To avoid vertical displacement of the entire graphene sheet, the position of one corner atom in the graphene sheet was fixed.

Nanopores were created by selectively removing atoms from the center of the graphene sheet. We considered ten pores with different sizes, which are named by the number of graphene ring units removed or partially opened, i.e., P-10, P-12, P-14, ..., P-28, as shown in Figures 1b–k, respectively. Every pore is characterized by an effective radius R_p given by $(A_p/\pi)^{1/2}$, where A_p is the effective pore area; the latter takes the finite size of carbon atoms on the pore rim into account and is calculated using hit-and-miss Monte Carlo integration as described in Supporting Information section 1.2.

Each MD simulation was run in the NVT ensemble for a period of 2×10^8 timesteps with a time step of 0.067 fs. The temperature was held constant at 300 K using a Nosé-Hoover thermostat. The interactions between C–C, H–H, and C–H were modeled by the AIREBO potential (see Supporting Information section 1.1.1), using the parameters specified within the LAMMPS package. The internal N_2 bond is modeled using a harmonic type potential (see Supporting Information section 1.1.3). All other interatomic interactions were modeled by the well-known Lennard-Jones potential (see Supporting Information section 1.1.2).

The flux through the membrane is calculated by averaging molecular crossings in both directions; as shown in section 3.1 of the Supporting Information, this is possible due to the lack of interactions between gas-phase molecules in the dilute gas limit. To further increase the number of crossings (samples) for a given simulation time, we have used a number of gas molecules that corresponds to a nominal gas pressure of 25.5 bar.

dx.doi.org/10.1021/la403969g | Langmuir 2014, 30, 675–682

Although this is significantly larger than the atmospheric pressure, we expect deviations from dilute-gas behavior to be small at this density ($n\sigma^3$ = 0.026, where n is the number density and σ is a nominal kinetic diameter). Comparison with simulations at 1, 10.1, and 41.2 bar nominal pressures shows differences to be small (see Supporting Information Figure 6). The agreement between two-sided equilibrium and one-sided nonequilibrium flux measurements shown in section 3.1 of the Supporting Information also suggests that the assumption of dilute gas behavior is reasonable.

Adsorbed Layers. Some gases are strongly adsorbed onto graphene, thus forming an adsorbed layer that can contribute to the flux across the membrane. Figure 2a plots the probability density of finding molecules of each of the gases involved in this study as a function of the distance from the membrane (z = 0); methane and nitrogen feature strong adsorption layers, while helium and hydrogen are significantly less attracted by the graphene membrane.

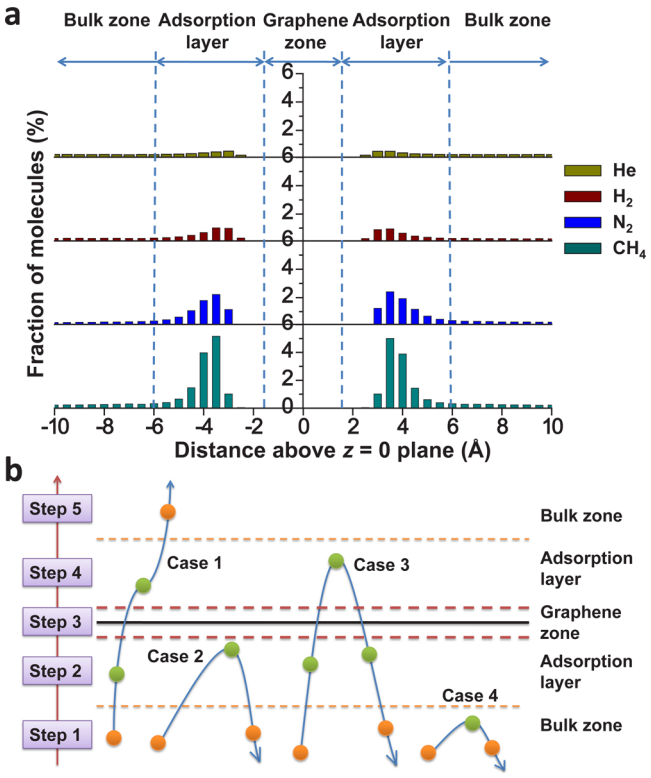

Figure 2. Adsorption onto the graphene surface and pore-crossing trajectories. (a) Probability density of gas molecules along the z-direction for He, H_2, N_2, and CH_4, respectively. Each simulation half is divided into three different zones (graphene zone, adsorption layer, and bulk zone) along the z-direction. (b) Typical pore-crossing trajectories. In case 1, a molecule crosses from the bulk on one side to the bulk on the other side. In case 2, a molecule visits the adsorption layer but returns to the bulk zone without crossing the pore. In case 3, a molecule crosses from one side to the other side but returns to the original side without entering the bulk zone of the opposite side. In case 4, molecules remain in the bulk. Orange denotes the initial or final position, while green denotes molecule in motion.

In order to analyze the relative contribution of the bulk (gas phase) and adsorbed layer to the flux across the membrane, we divide each simulation half into three different zones along the z-direction, namely the graphene zone, the adsorption layer, and the bulk zone (gas phase). The graphene zone is occupied by the graphene membrane of nominal width 0.34 nm. By observing that the gas density typically decays to its gas-phase value for (approximately) $|z| > 0.6$ nm, we define the adsorption layers as the regions 0.17 nm < $|z|$ < 0.6 nm as shown in Figure 2a. Using this notation, gas−membrane interaction can be described by breaking down gas−molecular motion into the four cases summarized in Figure 2b. In the present work the permeate flux across the membrane is comprised only of case 1 events (in both directions); that is, a molecule is considered to have crossed the graphene membrane if it moves from the bulk phase on one side to the bulk phase on the other side of the membrane. As discussed in section 2.2 of the Supporting Information, inclusion of case 3 events results in a difference in the molecular flux on the order of 7% for methane permeating the biggest pore (P-28). Because methane features the densest adsorbed layer, this amount is expected to be an upper bound on the discrepancy between the two definitions.

Due to the adsorption of molecules on the graphene surface, the equilibrium gas-phase density is expected to be, in general, not equal to the nominal gas density; the latter is defined as the number of gas particles divided by the volume of the simulation box excluding the volume of the graphene zone. This effect was taken into account in our results: the gas density was calculated by considering only the particles in the bulk region ($|z| > 0.6$ nm) and the volume available to them. This correction resulted in a reduction from the nominal simulation pressure of 25.5 bar by 0.4%, 3.4%, 12.2%, and 23.9% for He, H_2, N_2, and CH_4, respectively. The gas pressure was calculated using the ideal gas equation of state; comparison with the NIST standard reference program data reveals that use of the equation of state incurs a maximum error of approximately 4% for CH_4, while errors for the other gases are on the order of 1%.

Direct and Surface Flux. To elucidate the contribution of the bulk and surface mechanisms to the molecule permeation, we separate the total flux into two parts, namely the direct flux, in which the molecules cross directly from the bulk phase of one side to the bulk phase of the other side of the graphene, and the surface flux, in which the molecules cross after being adsorbed onto the graphene. A schematic illustration of the surface flux and direct flux definitions is shown in Figure 3a.

The two fluxes are distinguished based on the maximum polar angle θ_μ at which one molecule can directly cross through the pore, determined by the molecule radius (R_m) and pore radius (R_p) as shown in Figure 3a. Molecules entering the pore at polar angles smaller than θ_μ *and* having trajectories with radii of curvature (R_c) larger than 2 nm are considered to be contributing to the direct flux; molecules entering with larger values of θ_μ and/or having trajectories with smaller radii of curvature are assigned to the surface flux. We note that the angle criterion is based on a two-dimensional simplification of the interaction between the pore and the molecule and neglects the circular shape of the pore as well as the azimuthal orientation of molecular trajectories (see Figure 7 of Supporting Information); as a result, the simulation results are expected to provide an overestimate of the direct flux (underestimate of the surface flux).

THEORETICAL MODEL

The potential application of graphene membranes to gas separation has led to a number of recent MD studies assessing the possibility of separation by size exclusion. Surprisingly, the permeances reported in these studies exhibit significant variability with relative discrepancies up to 2 orders of

dx.doi.org/10.1021/la403969g | Langmuir 2014, 30, 675−682

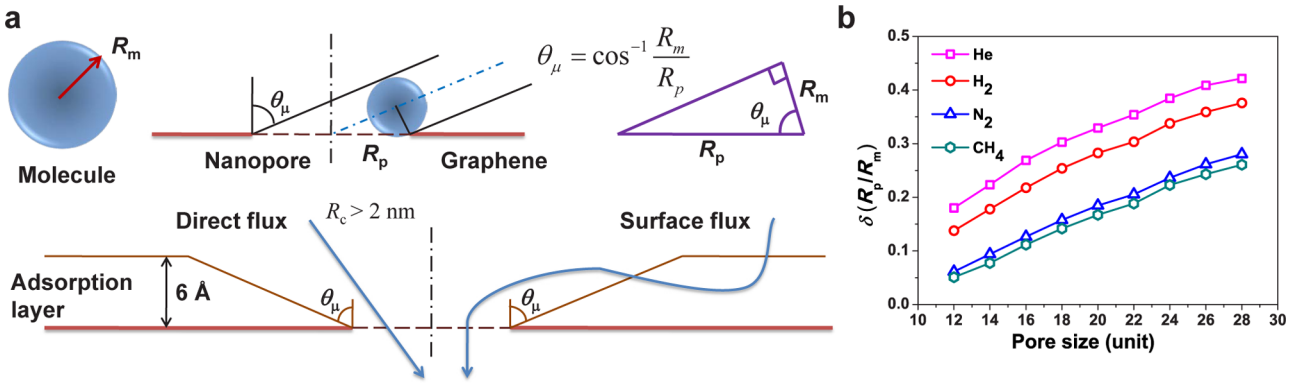

Figure 3. Regime and prediction of the direct flux. (a) Schematic illustration of the surface flux and direct flux. In our simulation the two types of crossing are separated by comparing the polar angle at which the molecule crosses the pore to the maximum angle θ_μ as well as the curvature of the molecular path in the adsorption layer. (b) $\delta(R_p/R_m)$ for He, H_2, N_2, and CH_4 permeating different pores.

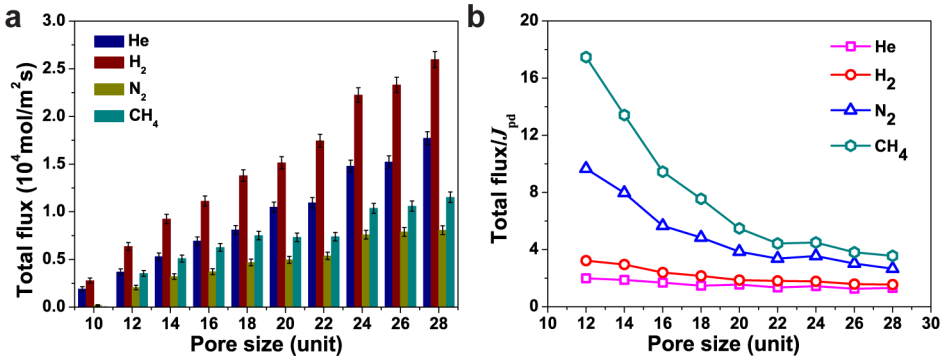

Figure 4. Permeate flux of the four different gases. (a) Permeate flux in units of mol/(m^2 s) through different pores for H_2, He, N_2, and CH_4. (b) Ratios of the total flux to the predicted direct flux.

magnitude for the same or similar pores. In order to validate our results, but also to provide a robust framework for estimating molecular fluxes through NPG membranes, we have developed a model for predicting the permeance of various NPG membranes as a function of the pore size and the gas kinetic diameter. This model is based on kinetic theory arguments for the molecular flux arriving at the pore from the bulk (gas) phase and does not account for the flux due to molecules adsorbed on the graphene surface.

The direct one-sided flux of point particles through a surface in an ideal gas can be calculated exactly at equilibrium and is given by

$$J = \frac{P}{\sqrt{2\pi RMT}} \tag{1}$$

where T is the gas temperature, R is the universal gas constant, M is the molar mass, and P is the gas pressure. By superposing the flux in both directions, this result can be used to describe the net flux of an ideal gas through an orifice that is much smaller than the gas mean free path in the presence of a pressure difference (ΔP), provided small deviations from equilibrium prevail.[42] This condition is satisfied by our simulations (see Supporting Information section 3.1) and is also expected to be satisfied in practical applications of interest. Therefore, for a membrane of area A_s, with a pore of effective area $A_p = \pi R_p^2$, the net ideal gas flux based on the membrane area is given by

$$J_{IG} = \frac{A_p}{A_s}\frac{\Delta P}{\sqrt{2\pi RMT}} \tag{2}$$

Molecule−pore interactions are incorporated by assuming that they are purely steric and that gas molecules behave as hard spheres of known kinetic diameters. Under these assumptions, the predicted direct gas flux is given by

$$J_{pd} = J_{IG}\delta(R_p/R_m) \tag{3}$$

The reduction in molecular flux due to steric considerations ($\delta(R_p/R_m) \leq 1$) can be calculated by finding the fraction of trajectories with molecular centers that intersect the graphene membrane within the pore diameter but cannot permeate the pore. This fraction was evaluated by simulating a large number of such trajectories using a Monte Carlo method described in more detail in section 4 of the Supporting Information. The resulting reduction in flux due to steric considerations for various gases and pore sizes is shown in Figure 3b.

We finally note that in our equilibrium simulations, instead of subtracting the two fluxes in opposite directions ($\Delta P = P - P = 0$), we add them to obtain twice the one-sided flux ($\Delta P = 2P$), as noted in the Simulation Method section and elaborated in section 3 of the Supporting Information.

RESULTS AND DISCUSSION

Selectivity. Figure 4a shows our MD results for the total flux (in units of mol/(m^2 s) based on the graphene surface area) through NPG membranes featuring the pores shown in Figures 1b−k. As expected, the flux of a given gas increases as

dx.doi.org/10.1021/la403969g | Langmuir 2014, 30, 675−682

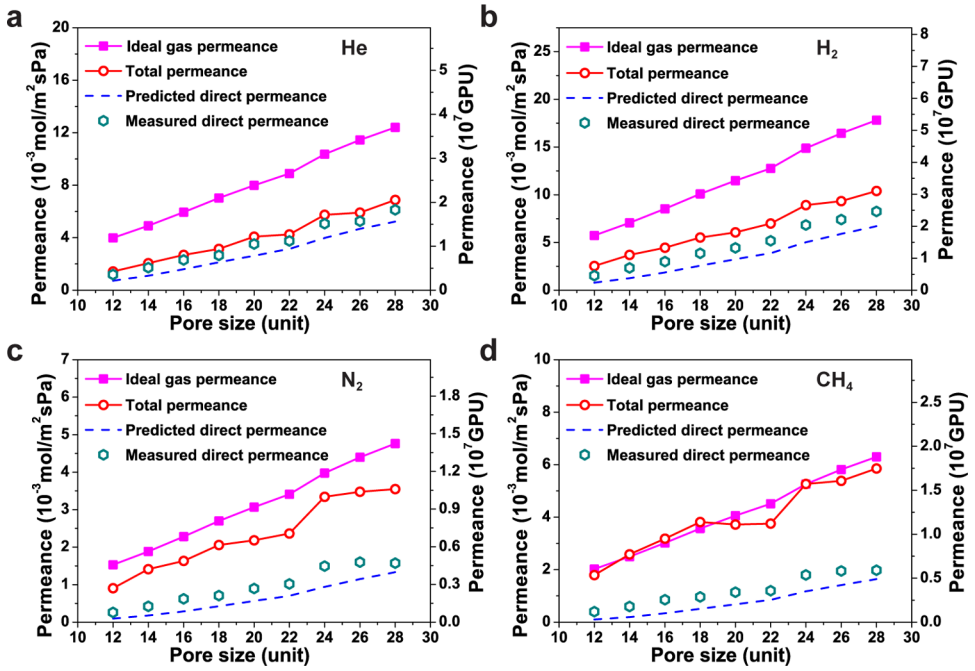

Figure 5. Comparison among different permeances for permeable pores. (a–d) Ideal gas permeance, total permeance, predicted direct permeance, and measured direct permeance through pores permeable to all gases considered (i.e., P-12, P-14, ..., and P-28) for He, H_2, N_2, and CH_4, respectively.

the pore size increases, while for a given pore size, the flux depends on the molecule kinetic diameter and mass as well as the strength of its interaction with the graphene surface. Transport rates through permeable pores are analyzed in more detail below; comparison with experimental results can be found in Figure 6.

Here we note that the simulation results show that pore P-10 is not permeable to methane, is very weakly permeable to nitrogen, and is significantly more permeable to hydrogen and helium (see Figure 4a). Specifically, during the simulation, no methane crossing events were observed (in the case of zero crossings an upper bound on the flux is estimated using a 95% Poisson[43] confidence interval), while the number of nitrogen crossing events was nonzero but an order of magnitude smaller than those observed for hydrogen and helium. This suggests that selective membranes are indeed possible if pores of this size and purity (no functionalization) can be reliably generated.

Modes of Transport. Figure 4b shows a comparison between the fluxes through various pores for the four gases considered in this study. The flux is normalized by the direct flux predicted by the theoretical model described in the previous section (eq 3). For gases that do not adsorb onto graphene (e.g., He and H_2), the ratio of total flux to predicted direct flux is close to 1; deviations from 1 arise due to the existence of a small surface flux and also due to the error associated with our kinetic theory model (e.g., the assumption of steric interactions and the use of a circular approximation for the pore geometry).

On the other hand, for gases that strongly adsorb onto the membrane (e.g., CH_4 and N_2) this ratio is generally larger than 1, clearly highlighting the importance of surface flux. We also observe that this ratio decreases as the pore size increases; for small pores this ratio becomes particularly large. This behavior can be explained by noting that the surface flux is expected to scale as R_p, while the direct flux scales as R_p^2; as $R_p \to 0$, the surface flux is expected to dominate the direct flux, while as R_p increases the contribution of the surface flux becomes increasingly less important. However, it is important to note that our simulations were effectively run at constant pore number density, thus contributing to this result, since as the pore diameter increases the graphene surface area available for adsorption decreases.

Transport across permeable pores is further analyzed for all gases considered in Figures 5a–d, which show the ideal gas permeance, total permeance, measured direct permeance, and predicted direct permeance for He, H_2, N_2, and CH_4. The figures show that the measured direct flux agrees well with the predicted direct flux, especially after recalling that the method for classifying direct and indirect crossing events used here provides an overestimate of the direct flux. We note that eq 3 predicts that *for a given pore size and permeating molecule* the permeance due to the kinetic part of the transport, $J_{pd}/\Delta P$, is proportional to the pore density; this may be important for comparing MD simulation results that are typically performed at different pore densities.

Pore Functionalization. Comparison of our results with the experimental data for the "Bi-4.9 Å" membrane by Koenig et al.[11] (Figure 6a) shows that our MD results predict leak rates that are approximately 2 orders of magnitude larger than the experimental results. The exception to this rule is transport of N_2 and CH_4 through the 10-unit pore (P-10), which was found to be selective (see section Selectivity). More precisely, the observed number of crossings for N_2 is within the experimentally observed range, while no CH_4 crossings were observed in our MD simulation, resulting in a 95% confidence interval for the leak rate of the gas that includes the experimentally observed range. We also observe that the ratio of experimental leak rates of permeable (H_2) to nonpermeable gases (N_2 and CH_4) is smaller than the corresponding simulated (P-10) results. This suggests that additional effects, not included in the simulations, are present in the experiments.

This observation, coupled to the fact that our results are in good agreement with theoretical (kinetic theory) estimates, leads us to believe that this discrepancy is due to pore

dx.doi.org/10.1021/la403969g | *Langmuir* 2014, 30, 675–682

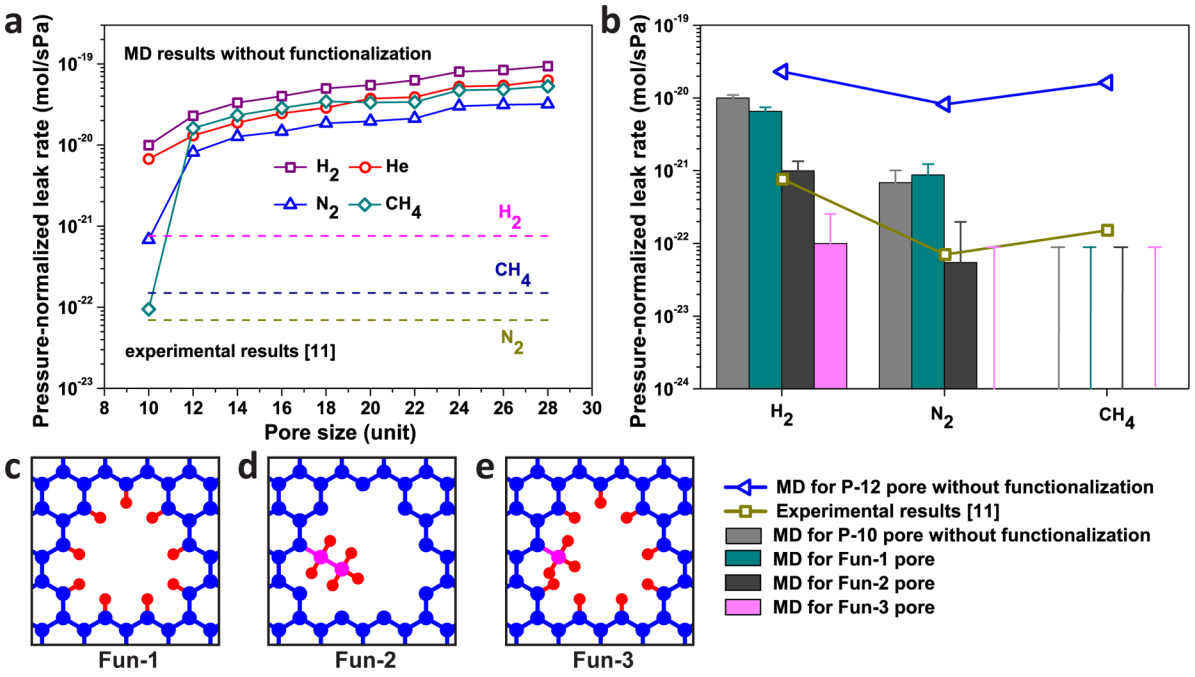

Figure 6. Effects of pore functionalization and comparison with experimental results. (a) Comparison of MD results for pores without functionalization with existing experimental results. The P-10 CH_4 data point denotes a 95% confidence upper bound on zero observed crossings. (b) Comparison of MD results for four selected pores (P-10, Fun-1, Fun-2, and Fun-3) with existing experimental results. MD results for pore P-12 without functionalization are also included. The uncertainty associated with the leak rate with no observed crossings is estimated based on a 95% Poisson confidence interval (see Supporting Information section 3.2). (c–e) Sketches of the functionalized pores Fun-1, Fun-2, and Fun-3, respectively. Blue spheres denote C atoms in graphene, red spheres denote H atoms, and pink spheres denote C atoms in the functional groups.

functionalization, which is expected to be present in membranes used in experiments. To validate this hypothesis, we performed simulations using 3 model functionalized 12-unit pores (denoted Fun-1, Fun-2, and Fun-3 in Figures 6c–e). Fun-1 corresponds to a single hydrogen atom added to each carbon atom on the pore rim; Fun-2 corresponds to a single ethyl group added to one location on the pore rim; Fun-3 corresponds to a single methyl group added to one location on the pore rim and single hydrogen atoms added to the other pore-rim carbon atoms. We chose ethyl and methyl groups to partly occlude the pore because they can be reliably modeled using the AIREBO potential, whereas modeling other chemical groups is more *ad hoc*.

Figure 6b gives a comparison of simulation results for 4 pores (P-10, Fun-1, Fun-2, and Fun-3) with experimental results; the figure also includes simulation results for the P-12 pore without functionalization. This figure shows that pore Fun-2 produces leak rates that are most consistent with the experimental results both in terms of overall fluxes and selectivity. In contrast, decreasing the pore size (P-10) results in similar nitrogen/hydrogen selectivity, but at much higher fluxes of hydrogen compared to the experimental results. The *relatively* high N_2 permeance observed in the case of pore Fun-2—despite a considerable effective area reduction, the permeance of N_2 through this pore is nonzero—may be a result of the flexibility of the functionalizing structure coupled with nitrogen's relatively large mass (compared to hydrogen).

CONCLUSIONS

We have shown that nanoporous graphene membranes can be used to separate gases with different kinetic diameters. Specifically, we have found a nanopore geometry that is permeable to hydrogen and helium, is significantly less permeable to nitrogen (selectivity >10), and is essentially impermeable to methane (selectivity >100). For the pore density of our simulations, the permeance of hydrogen and helium was on the order of 10^6 GPU, which is considerably higher than state-of-the-art polymer-based gas-separation membranes[14] and recently developed multilayer graphene oxide-based membranes.[44,45]

Molecule permeation through nanoporous graphene membranes is dependent not only on the molecule mass and kinetic diameter but also on the molecule adsorption on the graphene surface. The flux of molecules across the membrane can be decomposed into a direct part and a surface part. The direct flux can be estimated using kinetic theory provided steric considerations are taken into account. As expected, accounting for the molecule finite size reduces the predicted gas flow rate, especially for small pores ($\delta(R_p/R_m) \ll 1$ as $R_m/R_p \to 1$); as a result, for small pores the ideal gas flow rate (J_{IG}) strongly overestimates the direct flux and only becomes a reliable upper bound when the pore radius exceeds the nanometer scale.

The surface flux is negligible for gases that do not adsorb (e.g., He and H_2) onto graphene, while for gases that adsorb (e.g., CH_4 and N_2) it can be appreciable. In fact, for the latter, the contribution of surface flux is such that the total flux is on the same order of magnitude as the ideal gas flux (J_{IG}). Because of computational limitations, our MD simulations were performed at a high pore density which is expected to underestimate the effects of surface transport if the pore density is lower;[11,21,46] as a result, our comparison between direct and surface flux remains qualitative. A model is currently being developed to further quantify the contribution of surface adsorption to transport across graphene membranes.

Pore functionalization affects molecule permeation significantly and may be a contributing factor to the large discrepancy

dx.doi.org/10.1021/la403969g | *Langmuir* 2014, 30, 675–682

between simulated and experimentally measured transport rates through NPG membranes.

■ ASSOCIATED CONTENT

Supporting Information

Descriptions of the simulation method, detection of crossings, calculation of flux and permeance, and direct flux model are included. This material is available free of charge via the Internet at http://pubs.acs.org.

■ AUTHOR INFORMATION

Corresponding Author

*E-mail ngh@mit.edu (N.G.H.).

Notes

The authors declare no competing financial interest.

■ ACKNOWLEDGMENTS

This work was supported, in part, by the MITEI program and, in part, by the UniBSMIT-MechE faculty exchange Program cosponsored by the CARIPLO Foundation, Italy, under Grant No. 2008-2290. C.S. gratefully acknowledges financial support from the China Scholarship Council (CSC) for his study at the Massachusetts Institute of Technology. M.S.H.B. acknowledges financial (Fellowship) support from NSERC.

■ REFERENCES

(1) Allen, M. J.; Tung, V. C.; Kaner, R. B. Honeycomb Carbon: A Review of Graphene. *Chem. Rev.* **2009**, *110* (1), 132−145.

(2) Geim, A. K. Graphene: Status and Prospects. *Science* **2009**, *324* (5934), 1530−1534.

(3) Girit, Ç. Ö.; Meyer, J. C.; Erni, R.; Rossell, M. D.; Kisielowski, C.; Yang, L.; Park, C.-H.; Crommie, M. F.; Cohen, M. L.; Louie, S. G.; Zettl, A. Graphene at the Edge: Stability and Dynamics. *Science* **2009**, *323* (5922), 1705−1708.

(4) Balandin, A. A.; Ghosh, S.; Bao, W.; Calizo, I.; Teweldebrhan, D.; Miao, F.; Lau, C. N. Superior Thermal Conductivity of Single-Layer Graphene. *Nano Lett.* **2008**, *8* (3), 902−907.

(5) Chen, S.; Wu, Q.; Mishra, C.; Kang, J.; Zhang, H.; Cho, K.; Cai, W.; Balandin, A. A.; Ruoff, R. S. Thermal Conductivity of Isotopically Modified Graphene. *Nat. Mater.* **2012**, *11* (3), 203−207.

(6) Lee, C.; Wei, X.; Kysar, J. W.; Hone, J. Measurement of the Elastic Properties and Intrinsic Strength of Monolayer Graphene. *Science* **2008**, *321* (5887), 385−388.

(7) Geim, A. K.; Novoselov, K. S. The Rise of Graphene. *Nat. Mater.* **2007**, *6* (3), 183−191.

(8) Bunch, J. S.; Verbridge, S. S.; Alden, J. S.; van der Zande, A. M.; Parpia, J. M.; Craighead, H. G.; McEuen, P. L. Impermeable Atomic Membranes from Graphene Sheets. *Nano Lett.* **2008**, *8* (8), 2458−2462.

(9) Du, H.; Li, J.; Zhang, J.; Su, G.; Li, X.; Zhao, Y. Separation of Hydrogen and Nitrogen Gases with Porous Graphene Membrane. *J. Phys. Chem. C* **2011**, *115* (47), 23261−23266.

(10) Jiang, D.-e.; Cooper, V. R.; Dai, S. Porous Graphene As the Ultimate Membrane for Gas Separation. *Nano Lett.* **2009**, *9* (12), 4019−4024.

(11) Koenig, S. P.; Wang, L.; Pellegrino, J.; Bunch, J. S. Selective Molecular Sieving through Porous Graphene. *Nat. Nanotechnol.* **2012**, *7* (11), 728−732.

(12) Jiao, Y.; Du, A.; Hankel, M.; Smith, S. C. Modelling Carbon Membranes for Gas and Isotope Separation. *Phys. Chem. Chem. Phys.* **2013**, *15* (14), 4832−4843.

(13) Liu, H.; Dai, S.; Jiang, D.-e. Insights into CO_2/N_2 Separation through Nanoporous Graphene from Molecular Dynamics. *Nanoscale* **2013**, *5* (20), 9984−9987.

(14) Liu, H.; Dai, S.; Jiang, D.-e. Permeance of H_2 through Porous Graphene from Molecular Dynamics. *Solid State Commun.* **2013**, *175*−*176*, 101−105.

(15) Li, X.; Cai, W.; An, J.; Kim, S.; Nah, J.; Yang, D.; Piner, R.; Velamakanni, A.; Jung, I.; Tutuc, E.; Banerjee, S. K.; Colombo, L.; Ruoff, R. S. Large-Area Synthesis of High-Quality and Uniform Graphene Films on Copper Foils. *Science* **2009**, *324* (5932), 1312−1314.

(16) Kim, K. S.; Zhao, Y.; Jang, H.; Lee, S. Y.; Kim, J. M.; Kim, K. S.; Ahn, J.-H.; Kim, P.; Choi, J.-Y.; Hong, B. H. Large-Scale Pattern Growth of Graphene Films for Stretchable Transparent Electrodes. *Nature* **2009**, *457* (7230), 706−710.

(17) Novoselov, K. S.; Geim, A. K.; Morozov, S. V.; Jiang, D.; Zhang, Y.; Dubonos, S. V.; Grigorieva, I. V.; Firsov, A. A. Electric Field Effect in Atomically Thin Carbon Films. *Science* **2004**, *306* (5696), 666−669.

(18) Park, S.; Ruoff, R. S. Chemical Methods for the Production of Graphenes. *Nat. Nanotechnol.* **2009**, *4* (4), 217−224.

(19) Alemán, B.; Regan, W.; Aloni, S.; Altoe, V.; Alem, N.; Girit, C.; Geng, B.; Maserati, L.; Crommie, M.; Wang, F.; Zettl, A. Transfer-Free Batch Fabrication of Large-Area Suspended Graphene Membranes. *ACS Nano* **2010**, *4* (8), 4762−4768.

(20) Lin, Y.-C.; Jin, C.; Lee, J.-C.; Jen, S.-F.; Suenaga, K.; Chiu, P.-W. Clean Transfer of Graphene for Isolation and Suspension. *ACS Nano* **2011**, *5* (3), 2362−2368.

(21) O'Hern, S. C.; Stewart, C. A.; Boutilier, M. S. H.; Idrobo, J.-C.; Bhaviripudi, S.; Das, S. K.; Kong, J.; Laoui, T.; Atieh, M.; Karnik, R. Selective Molecular Transport through Intrinsic Defects in a Single Layer of CVD Graphene. *ACS Nano* **2012**, *6* (11), 10130−10138.

(22) Russo, C. J.; Golovchenko, J. A. Atom-by-Atom Nucleation and Growth of Graphene Nanopores. *Proc. Natl. Acad. Sci. U. S. A.* **2012**, *109* (16), 5953−5957.

(23) Bai, J.; Zhong, X.; Jiang, S.; Huang, Y.; Duan, X. Graphene Nanomesh. *Nat. Nanotechnol.* **2010**, *5* (3), 190−194.

(24) Bieri, M.; Treier, M.; Cai, J.; Ait-Mansour, K.; Ruffieux, P.; Groning, O.; Groning, P.; Kastler, M.; Rieger, R.; Feng, X.; Mullen, K.; Fasel, R. Porous Graphenes: Two-Dimensional Polymer Synthesis with Atomic Precision. *Chem. Commun.* **2009**, *45*, 6919−6921.

(25) Huh, S.; Park, J.; Kim, Y. S.; Kim, K. S.; Hong, B. H.; Nam, J. M. UV/Ozone-Oxidized Large-Scale Graphene Platform with Large Chemical Enhancement in Surface-Enhanced Raman Scattering. *ACS Nano* **2011**, *5* (12), 9799−9806.

(26) Liu, L.; Ryu, S.; Tomasik, M. R.; Stolyarova, E.; Jung, N.; Hybertsen, M. S.; Steigerwald, M. L.; Brus, L. E.; Flynn, G. W. Graphene Oxidation: Thickness-Dependent Etching and Strong Chemical Doping. *Nano Lett.* **2008**, *8* (7), 1965−1970.

(27) Sint, K.; Wang, B.; Král, P. Selective Ion Passage through Functionalized Graphene Nanopores. *J. Am. Chem. Soc.* **2008**, *130* (49), 16448−16449.

(28) Cohen-Tanugi, D.; Grossman, J. C. Water Desalination across Nanoporous Graphene. *Nano Lett.* **2012**, *12* (7), 3602−3608.

(29) Humplik, T.; Lee, J.; O'Hern, S. C.; Fellman, B. A.; Baig, M. A.; Hassan, S. F.; Atieh, M. A.; Rahman, F.; Laoui, T.; Karnik, R.; Wang, E. N. Nanostructured Materials for Water Desalination. *Nanotechnology* **2011**, *22* (29), 292001.

(30) Suk, M. E.; Aluru, N. R. Water Transport through Ultrathin Graphene. *J. Phys. Chem. Lett.* **2010**, *1* (10), 1590−1594.

(31) Wang, E. N.; Karnik, R. Water Desalination: Graphene Cleans Up Water. *Nat. Nanotechnol.* **2012**, *7* (9), 552−554.

(32) Hauser, A. W.; Schrier, J.; Schwerdtfeger, P. Helium Tunneling through Nitrogen-Functionalized Graphene Pores: Pressure- and Temperature-Driven Approaches to Isotope Separation. *J. Phys. Chem. C* **2012**, *116* (19), 10819−10827.

(33) Hauser, A. W.; Schwerdtfeger, P. Nanoporous Graphene Membranes for Efficient $^3He/^4He$ Separation. *J. Phys. Chem. Lett.* **2011**, *3* (2), 209−213.

(34) Schrier, J.; McClain, J. Thermally-Driven Isotope Separation across Nanoporous Graphene. *Chem. Phys. Lett.* **2012**, *521*, 118−124.

(35) Postma, H. W. C. Rapid Sequencing of Individual DNA Molecules in Graphene Nanogaps. *Nano Lett.* **2010**, *10* (2), 420−425.

(36) Schneider, G. G. F.; Kowalczyk, S. W.; Calado, V. E.; Pandraud, G. g.; Zandbergen, H. W.; Vandersypen, L. M. K.; Dekker, C. DNA Translocation through Graphene Nanopores. *Nano Lett.* **2010**, *10* (8), 3163−3167.
(37) Du, A.; Zhu, Z.; Smith, S. C. Multifunctional Porous Graphene for Nanoelectronics and Hydrogen Storage: New Properties Revealed by First Principle Calculations. *J. Am. Chem. Soc.* **2010**, *132* (9), 2876−2877.
(38) Shan, M.; Xue, Q.; Jing, N.; Ling, C.; Zhang, T.; Yan, Z.; Zheng, J. Influence of Chemical Functionalization on the CO_2/N_2 Separation Performance of Porous Graphene Membranes. *Nanoscale* **2012**, *4* (17), 5477−5482.
(39) Schrier, J. Carbon Dioxide Separation with a Two-Dimensional Polymer Membrane. *ACS Appl. Mater. Interfaces* **2012**, *4* (7), 3745−3752.
(40) Drahushuk, L. W.; Strano, M. S. Mechanisms of Gas Permeation through Single Layer Graphene Membranes. *Langmuir* **2012**, *28* (48), 16671−16678.
(41) http://lammps.sandia.gov, Sandia National Laboratories.
(42) Hasegawa, M.; Sone, Y. Rarefied Gas Flow through a Slit. *Phys. Fluids A* **1991**, *3* (3), 466−477.
(43) Hadjiconstantinou, N. G.; Garcia, A. L.; Bazant, M. Z.; He, G. Statistical Error in Particle Simulations of Hydrodynamic Phenomena. *J. Comput. Phys.* **2003**, *187* (1), 274−297.
(44) Kim, H. W.; Yoon, H. W.; Yoon, S.-M.; Yoo, B. M.; Ahn, B. K.; Cho, Y. H.; Shin, H. J.; Yang, H.; Paik, U.; Kwon, S.; Choi, J.-Y.; Park, H. B. Selective Gas Transport through Few-Layered Graphene and Graphene Oxide Membranes. *Science* **2013**, *342* (6154), 91−95.
(45) Li, H.; Song, Z.; Zhang, X.; Huang, Y.; Li, S.; Mao, Y.; Ploehn, H. J.; Bao, Y.; Yu, M. Ultrathin, Molecular-Sieving Graphene Oxide Membranes for Selective Hydrogen Separation. *Science* **2013**, *342* (6154), 95−98.
(46) Boutilier, M. S. H.; Sun, C.; O'Hern, S. C.; Au, H.; Hadjiconstantinou, N. G.; Karnik, R. Implications of Permeation through Intrinsic Defects in Graphene on the Design of Defect-Tolerant Membranes for Gas Separation. *ACS Nano*, DOI: 10.1021/nn405537u.